13th World Conference on Earthquake Engineering
Vancouver, B.C., Canada
August 1-6, 2004
Paper No. 1763

EARTHQUAKE RESISTANT PERFORMANCE AND FAILURE MECHANISM OF PRECAST PRESTRESSED CONCRETE BEAM-COLUMN JOINTS ASSEMBLED BY POST-TENSIONING STEEL BARS

Shinji KISHIDA [1], Kazuhiro KITAYAMA[2], Makoto MARUTA[3], Kensaku MORIYAMA[4]

SUMMARY

Prestressed concrete beam-column subassemblage specimens, which were prefabricated by passing post-tensioning tendons through precast RC beams and columns, were tested under reversed cyclic loading. Beam-column joint panel failed in shear for specimens provided bond between post-tensioning bars and concrete by grout injection, whereas concrete compressive failure due to flexural moment was observed at beam ends for unbonded specimen. To study on horizontal shear force input to joint panel, concrete compressive stress distribution acting on beam critical section was researched through measuring concrete normal strains by gauges stuck on beam surface. Central region of joint panel concrete in some height was subjected to horizontal compression by concrete stress blocks on beam critical sections on both sides of a joint. This means that all concrete compressive force at beam and column critical section is not necessarily introduced to a joint panel. The horizontal and vertical joint input shear force, which were computed using measured tensile forces of post-tensioning steel beam and column bars and accounting for non-contribution of the compressive force in middle region of a joint to horizontal and vertical shear respectively, deteriorated with the decrease in story shear force. Shear strength in interior beam-column joint obtained by above-mentioned method agreed well with average shear strength predicted by AIJ provision proposed for RC beam-column joints. The measured joint shear cracking strength was almost equal to two-thirds of the computed results based on the principal stress field taking account of the prestress to a beam.

INTRODUCTION

Shear strength in reinforced concrete (RC) beam-column joints can be obtained by Design Guidelines of Architectural Institute of Japan [1], which depends on both the joint shapes as interior, exterior or knee joint and the concrete compressive strength. Whereas, the strength in precast prestressed concrete beam-column joints assembled by post-tensioning steel bars called as PCaPC has not been estimated quantitatively. There are few test data on joint failure of PCaPC beam-column subassemblages [2].

[1] *Research Associate, Tokyo Metropolitan University, Tokyo, Japan. E-mail: skishida@ecomp.metro-u.ac.jp*
[2] *Associate Professor, Tokyo Metropolitan University, Tokyo, Japan. E-mail: kitak@ecomp.metro-u.ac.jp*
[3] *Kajima Technical Research Institute, Tokyo, Japan. E-mail: maruta@kajima.com*
[4] *Graduate School of Engineering, Tokyo Metropolitan University, Tokyo, Japan.*

Therefore PCaPC beam-column joint specimens were tested under reversed cyclic lateral loading and column axial loading to study the joint failure mechanism.

OUTLINE OF TEST

Specimens

Properties of specimens are summarized in Table 1. Section dimensions and reinforcement details are shown in Fig.1. Seven plane cruciform subassemblage specimens and one exterior beam-column joint specimen with two-fifth scale to actual frames were tested. Beam and column elements were precast separately. Post-tensioning steel bars with deformed surface or wire strands were used to connect precast RC beams and column. Therefore beam longitudinal bars were terminated at column face. Interface mortal with the width of 20mm was set between precast beam and column. Bond along post-tensioning tendons were provided by injecting grout mortal into the sheath except for Specimen BNU. The column section was square with 350mm depth. The depth and width of a beam section was 400mm and 250mm, respectively. Two sets of 2-D10 were arranged in a beam-column joint region as the lateral reinforcement for all specimens. The length from the center of column to the pin-roller support of beam end was 1600mm. The height from the center of beam to the loading point on the top of the column or to the bottom support was 1415mm. The shear span ratio were 4.0 in the column and 4.3 in the beam, respectively.

Specimen BNN1 was the control specimen. Normal strength mortal was used for grout into the sheath and vertical joint adjacent to column face for Specimens BNN1, WNN and BNN2. Prestressing strands were used for Specimen WNN. Initial tensile force imposed to post-tensioning steel bars in Specimen BNN2 was almost the half of the control Specimen BNN1. Unbonded post-tensioning steel bars were used for Specimen BNU. High strength mortal for grout into the sheath and fiber mortal for vertical joint adjacent to column face were used for Specimen BFH. High strength mortal was used for grout into the sheath and for vertical joint adjacent to column face for Specimens BHH1, BHH2 and BHH3. Specimens BNN1, WNN, BNU, BNN2, BHH1 and BFH were designed to develop beam yielding. Specified concrete compressive strength of 30MPa for a column and the diameter of 36mm for a post-tensioning steel bar passing through beams were chosen to cause joint shear failure for Specimens BHH2 and BHH3. The

Table 1 Properties of Specimens

Specimens		BNN1	WNN	BNU	BNN2	BHH1	BFH	BHH2	BHH3
Prestressing Steel Bars		2-D32	Prestressing Strand*1	2-D32				2-D36	
Concrete Compressive Strength	Column	73.3	75.5	76.6	76.1	77.2	77.7	43.0	39.9
	Beam							71.7	67.4
Column Axial Load (Compression, stress ratio)		937kN (0.13)						469kN (0.13)	
Mortal of Vertical Joint		Normal Strength				High	Fiber*2	High Strength	
Grout		Normal Strength		None	Normal	High Strength			
Shape of Subassemblage		Interior Beam-Column Joint							Exterior
Ratio of Tensile Force to Yield Strength		0.7			0.4	0.7			
Steel Factor*3		0.279	0.143	0.279				0.345	
Column Longitudinal Bars		4-D32 (SBPR 930/1080)							
Joint Lateral Bars		2-D10 2 sets							

D32 (SBPR 930/1080) : Sheath-49mm, D36 (SBPR 930/1080) : Sheath-56mm, 12.4A (SWPR 7A) : Sheath-56mm

*1 Prestressing Strand : 5 -ϕ12.4

*2 Fiber : PVA (Polypropylene)

*3 Steel Factor : $q = \frac{a_y \cdot \sigma_y + a_{py} \cdot \sigma_{py}}{bD \cdot \sigma_B}$, where, a_y : Section Area of Longitudinal Bar, σ_y : Yield Strength of Longitudinal Bar, a_{py} : Section Area of PC Bar, σ_{py} : Yield Strength of PC Bar, b : Width of Section, D : Depth of Section, σ_B : Concrete Compressive Strength

Table 2 Material properties of joint mortal

Joint Mortal		Compressive Strength, MPa	Secant Modulus, GPa	Tensile Strength, MPa
Normal	BNN1	62.1	21.0	4.37
	WNN	63.5	22.0	
	BNU	64.9	22.0	
	BNN2	64.2	22.0	
Fiber	BFH	66.5	20.3	-
High	BHH1	105.3	39.1	4.07
	BHH2	101.8	37.0	
	BHH3	100.1	36.1	

Table 3 Material properties of grout

Grout		Compressive Strength, MPa	Secant Modulus, GPa	Tensile Strength, MPa
Normal	BNN1	51.1	13.2	1.79
	WNN	51.1	13.4	
	BNN2	51.4	13.7	
-	BNU	-	-	-
High	BHH1	118.3	32.5	4.91
	BFH	119.3	32.6	
	BHH2	112.0	31.9	
	BHH3	109.2	31.6	

Table 4 Material properties of concrete

Specimens	Compressive Strength, MPa	Strain at Maximum Strength, %	Secant Modulus, GPa	Tensile Strength, MPa
BNN1	73.3	0.254	40.3	4.45
WNN	75.5	0.255	41.0	
BNU	76.6	0.258	41.1	
BNN2	76.1	0.256	41.0	
BHH1	77.2	0.260	41.1	
BFH	77.7	0.262	41.1	
BHH2*1	43.0	0.216	33.1	2.99
	71.7	0.255	39.7	4.45
BHH3*1	39.9	0.212	32.2	2.99
	67.4	0.257	38.0	4.45

*1 Upper column:concrete of column , Lower column: concrete of beam

Table 5 Material properties of steel bars

Diameter		Yield Strength, MPa	Young's Modulus, GPa	Yield Strain, %
D32	BNN1	1014.4	195.1	0.720*1
	BNU			
	BNN2			
	BHH1			
	BFH			
5-φ12.4	WNN	1794.8	22.0	1.017
D36	BHH2	1023.6	211.1	0.685*1
	BHH3			
Column Longitudinal Bar (D32)		1014.4	195.1	0.720*1
Reinforcing Bar (D10)		418.7	187.0	0.225

*1 Yield strain determined nominally by 0.2% offset meth

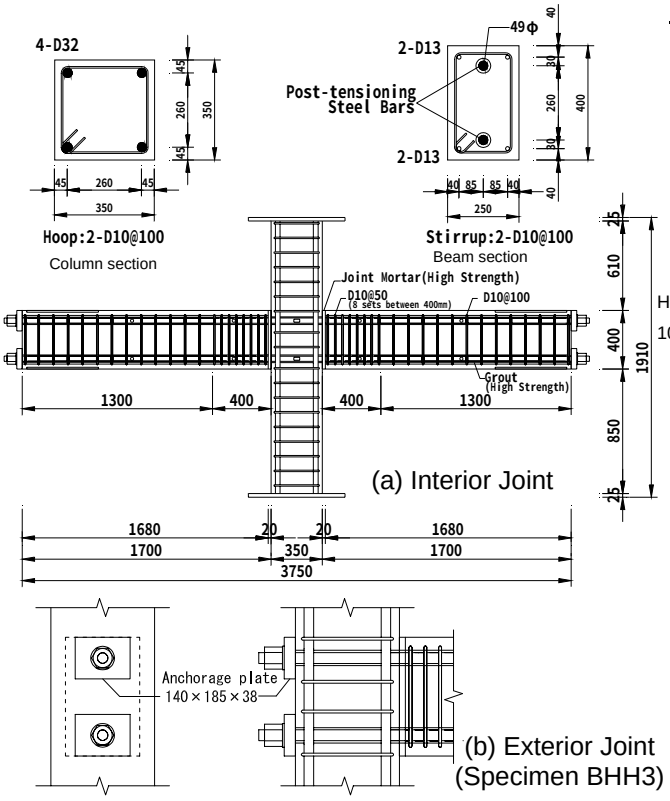

Fig.1 Section dimensions and reinforcement details

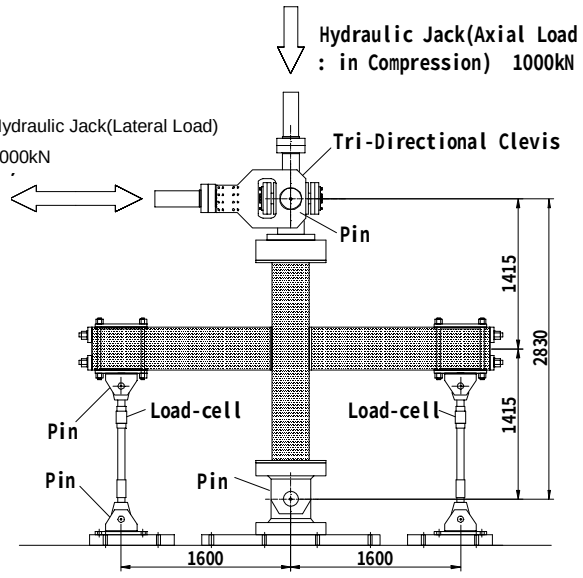

Fig.2 Loading apparatus

volume of the stirrup in beam hinge regions was increased to two times more than that in elastic region. Specimen BHH3 is the exterior beam-column joint. The post-tensioning steel beam bars were anchored with the anchor plates outside the column face (see Fig.1 (b)). Material properties of concrete, mortal, grout and steel are listed in Tables 2, 3, 4 and 5.

Loading Methods and Instrumentation

The loading system is shown in Fig.2. The beam ends were supported by horizontal rollers, while the bottom of the column was supported by a mechanical hinge. The reversed horizontal load and the constant axial load in compression were applied at the top of the column. All Specimens were controlled by the story drift angle for one cycle of 1/400, two cycles of 1/200 and 1/100, one cycle of 1/66, two cycles of 1/50, one cycle of 1/33 and two cycles of 1/25. The lateral force applied to the top of a column, the column axial load and the shear forces of both beam ends were measured by load-cells. The story drift, beam and column deflections, and local displacement of a joint panel were measured by displacement transducers. The strains of prestressing tendons, beam bars, column bars and the joint lateral reinforcement were measured by strain gauges. Moreover, concrete strain distribution at the beam end adjacent to column face was measured by concrete strain gauges attached on concrete surface (see Fig.6).

TEST RESULTS

Crack Pattern and Failure Mode

Crack patterns at the end of test are shown in Fig.3. Flexural cracks in beams and column and diagonal shear cracks in a joint panel were observed for all specimens. The column longitudinal bars did not yield. Joint lateral reinforcement yielded for all specimens at the story drift angle of 1.0%. Post- tensioning steel bars passing through beams yielded for Specimens BNN1, BNN2, BHH1 and BFH. On the contrary, for other specimens post-tensioning steel bars of the beam did not yield. Diagonal joint shear cracks expanded considerably except for Specimen BNU. The shell concrete spalled off in a joint panel. The

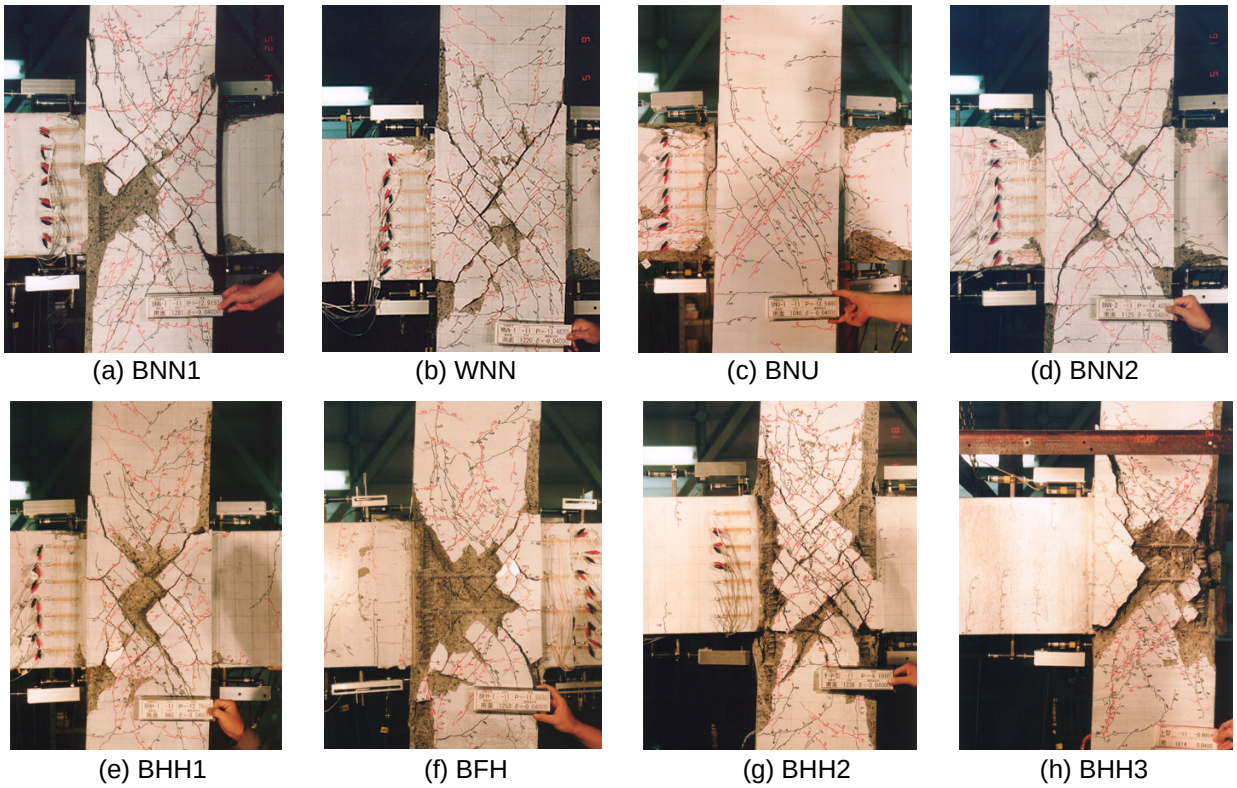

(a) BNN1 (b) WNN (c) BNU (d) BNN2

(e) BHH1 (f) BFH (g) BHH2 (h) BHH3

Fig.3 Crack patterns at end of test

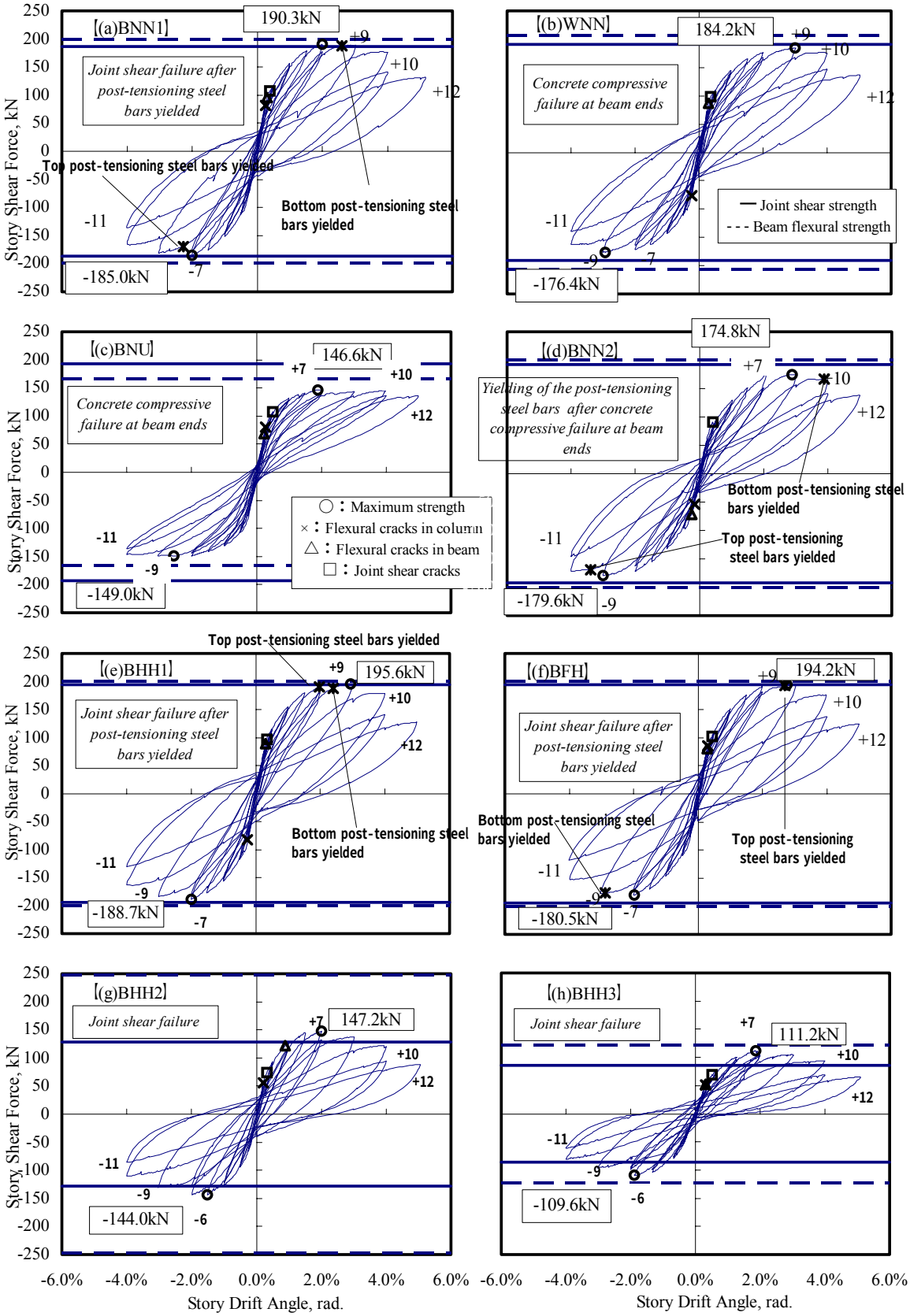

Fig.4 Relationship between story shear force and story drift

diagonal cracks were not observed in beams for all specimens. Concrete crushing at beam ends occurred for Specimen BNU without wide opening of joint shear cracks. It was concluded that Specimens BHH2 and BHH3 failed in joint shear, Specimens BNU and WNN failed by concrete crushing at beam ends in bending moment, Specimen BNN2 failed by yielding of the post-tensioning steel bars after concrete crushing at beam ends in bending moment and Specimens BNN1, BHH1 and BFH failed eventually in joint shear after the post-tensioning steel bars yielded.

Story Shear - Drift Relationship

The story shear force - story drift relationships are shown in Fig.4. The story shear force was computed from moment equilibrium between measured beam shear forces and the horizontal force at the loading point on the top of the column. The occurrence of flexural cracking in beams and column, diagonal shear cracking in a joint panel and yielding of post-tensioning steel bars are marked in Fig.4. The joint shear strength computed according to Reference [1] and beam flexural strength are shown by a solid line and a dashed line respectively in Fig.4. The lever arm lengths between tensile resultant force and concrete compressive force on beam and column section were assumed to be 289mm and 267mm respectively when converting joint shear strength to story shear force. Beam flexural strength was calculated according to the section analysis on the basis of the assumption that plane sections remain plane. The story shear reached the maximum force at the story drift angle of 1.5% for Specimen BHH3, 2% for Specimens BNN1 and BHH2 and 3% for other specimens. The measured maximum story shear for Specimens BHH2 and BHH3 was larger than the calculated joint shear strength, whereas that for other specimens was smaller than the calculated joint shear strength. The story shear force decreased gradually after story shear force reached the maximum value. The measured maximum story shear for Specimens BNN1, BHH1 and

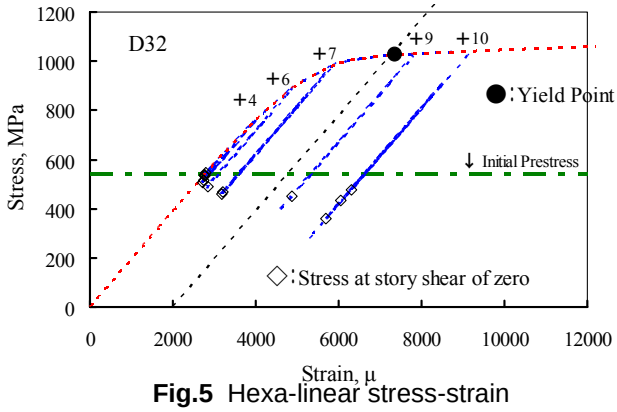

Fig.5 Hexa-linear stress-strain relationship model

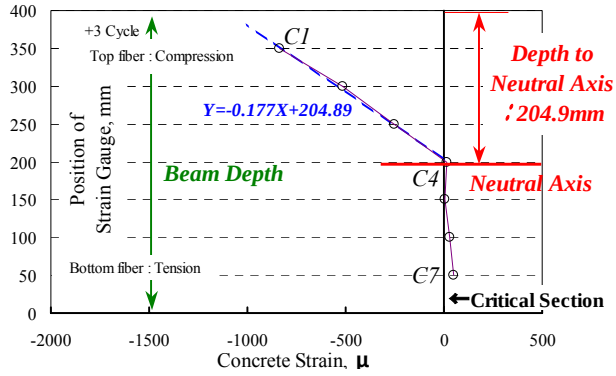

Fig.7 Method for deciding the beam neutral axis position

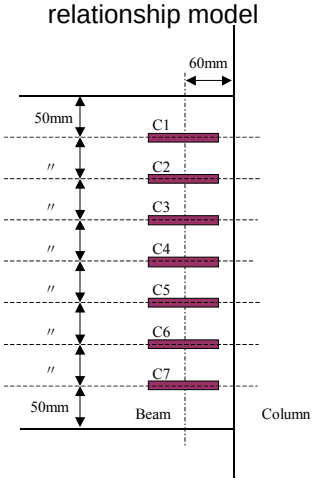

Fig.6 Location of concrete gauges on beam surface

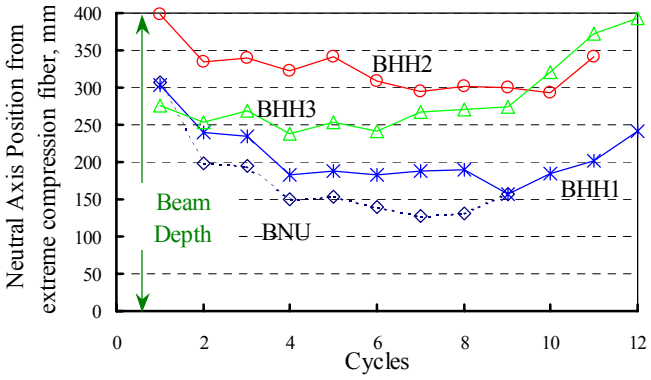

Fig.8 Transitions of the neutral axis position

BFH coincided with the story shear force corresponding to calculated beam flexural strength. Specimen BNU which used unbonded post-tensioning steel bars showed the hysteresis characteristic of directing to the origin point as conventional PC assemblages. Other specimens exhibited origin-oriented loops at first, but gradually showed spindle-shaped hysteresis loops with the increase in story drift and resembled histeresis characteristic of RC assemblage.

DISCUSSIONS OF TEST RESULTS

The stresses of post-tensioning steel bars used in the paper were obtained from strains measured by strain gauges through hexa-linear stress-strain relationship model as shown in Fig.5, where stress of the deformed post-tensioning steel bar with the diameter of 32mm was traced as an instance with measured strain.

Transition of Neutral Axis Depth

Concrete strain gauges as shown in Fig.6 were attached on the surface of a beam at the location of 60mm apart from a beam critical section. Change of the neutral axis position on a beam critical section was investigated by using concrete strain distribution. Method for deciding the beam neutral axis position is explained for example by Fig.7. Measured strain distribution at the location of C1 from C4, excluding strains at the location of C5 from C7, was approximated by the line induced from least squares method. Hence the neutral axis position was decided as the point at which obtained strain line crosses the vertical axis. The shape of concrete compressive stress block is assumed to be triangular as shown in Fig.7.

Transitions of the neutral axis position are shown in Fig.8 for four specimens. The neutral axis depth for Specimens BHH2 and BHH3 which failed in joint shear was greater than the half of beam depth, i.e., 200mm from the extreme compression fiber during tests. In other words central region of joint panel concrete in some height was subjected to horizontal compression by concrete stress blocks on beam critical sections on both sides of a joint panel as shown in Fig.10 (b). This means that all concrete compressive force at beam critical section was not necessarily introduced to a joint panel as a horizontal shear. The neutral axis approached to the extreme compression fiber with the increase in deformation.

Joint Input Horizontal Shear Force

Envelope curves of relationship between joint shear stresses and shear distortion are shown in Fig.9 by dotted lines. The joint shear average and lower strengths calculated according to AIJ provisions [1] are also shown by a horizontal chain line and two-dot chain line respectively. Joint input shear force denoted as V_{jh} was computed from post-tensioning steel bar stresses by Equations (1) or (2) according to the definition shown in Fig.10. Sectional area effective to horizontal joint shear force was assumed as the product of column depth and the average of beam and column width when joint input shear force was transformed into shear stress. As mentioned above, it is necessary to consider two cases; one is 1) that the distance from the extreme compression fiber to neutral axis (depth of compressive stress distribution) is less than the half of beam depth as illustrated in Fig.10 (a), and the other is 2) that it is greater than the half of beam depth as illustrated in Fig.10 (b). In the second case, the maximum joint shear input force can be obtained mathematically along horizontal section at the center of joint depth. Therefore joint input shear force was computed as Equation (2).

1) In case that depth of compressive stress block is less than the half of beam depth;

$$V_{jh}=P_{t1}+P_{b2}-V_c \quad (1)$$

2) In case that depth of compressive stress block denoted as a_b in Fig.10 (b) is greater than the half of beam depth;

$$V_{jh}=\alpha_1 C_{c2}-P_{t2}+P_{t1}-\alpha_2 C_{c1}-V_c \quad (2)$$

$$C_{c1}=P_{t1}+P_{b1} \quad (3)$$

$$C_{c2}=P_{t2}+P_{b2} \quad (4)$$

$$\alpha_1=1-\alpha_2 \quad (5)$$

$$\alpha_2=(a_b-D/2)^2/\, a_b{}^2 \qquad (\alpha_1+\alpha_2=1) \quad (6)$$

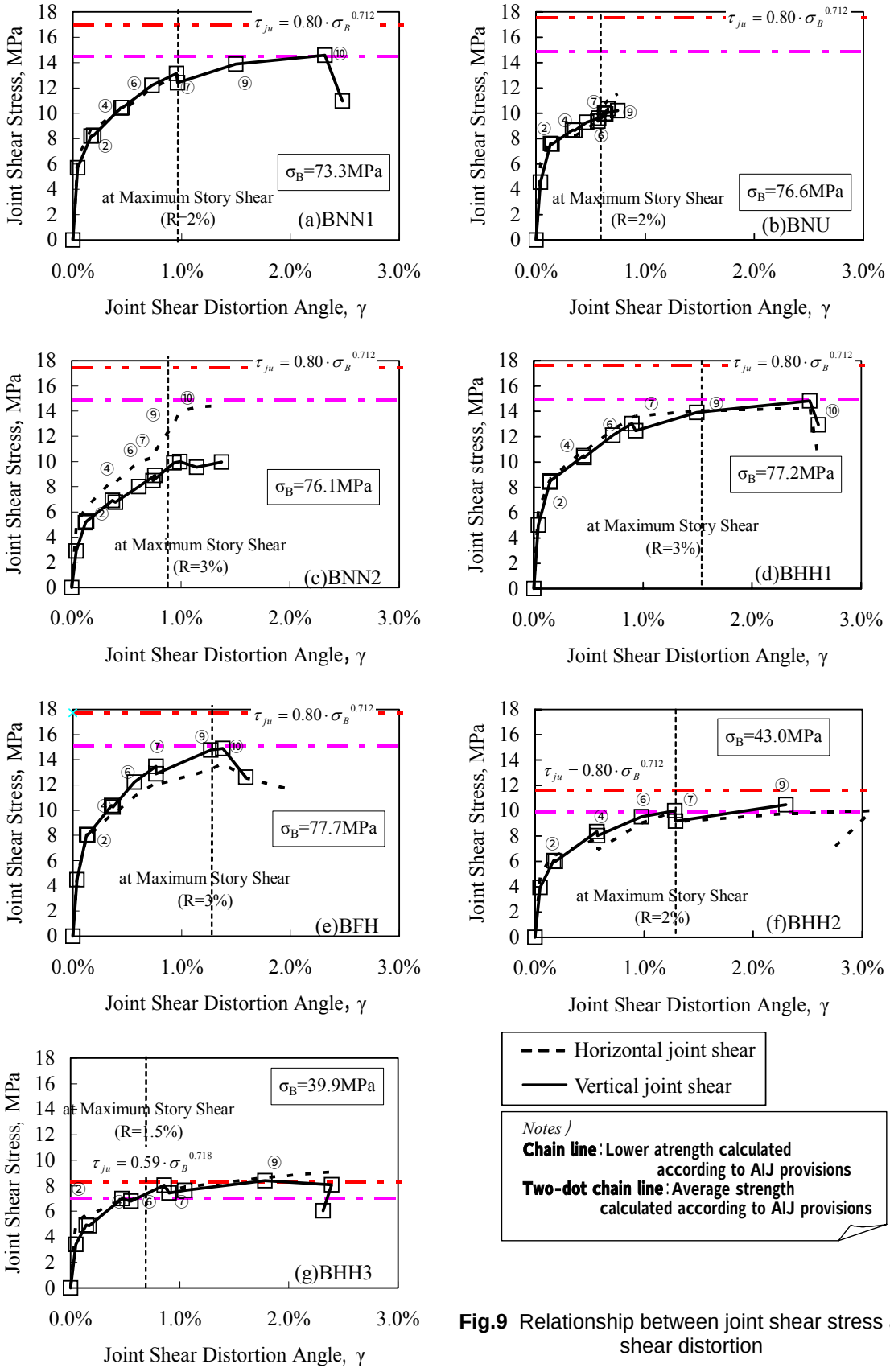

Fig.9 Relationship between joint shear stress and shear distortion

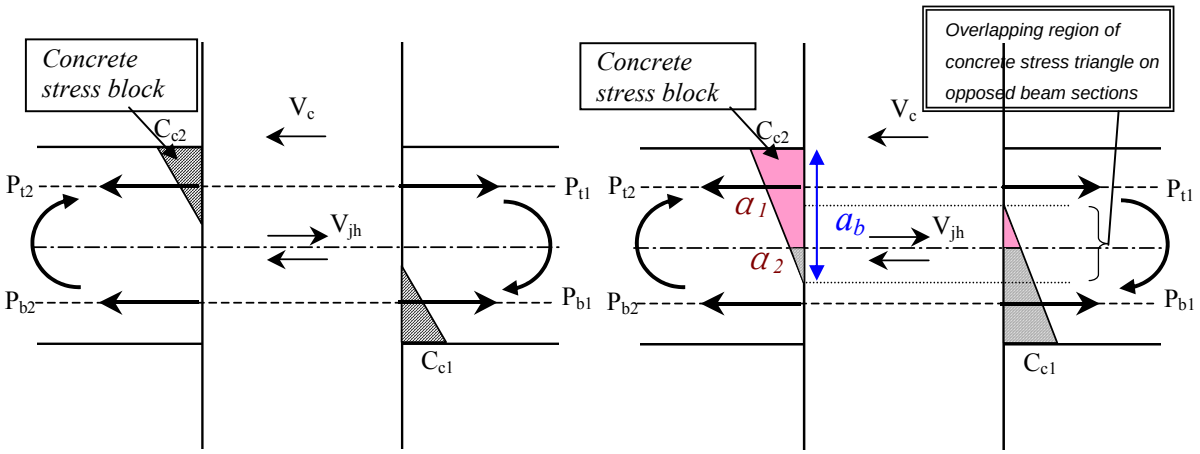

(a) In case that depth of compressive stress block is less than the half of beam depth

(b) In case that depth of compressive stress block is greater than the half of beam depth

Fig.10 Stress acting on joint panel (Lateral direction)

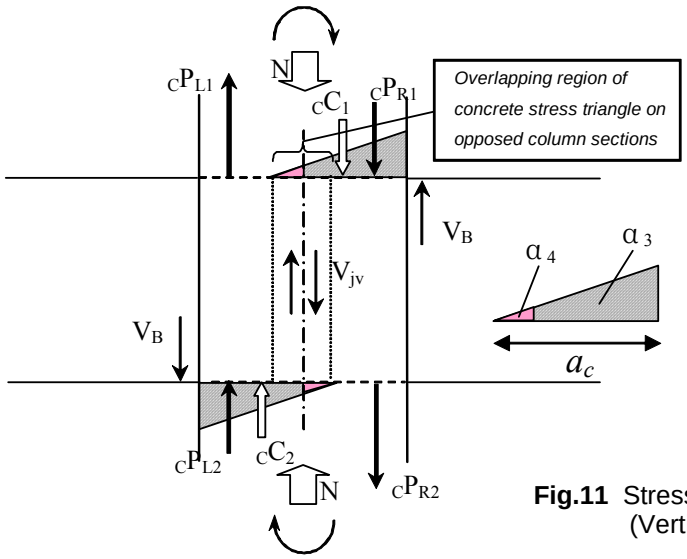

Fig.11 Stress acting on joint panel (Vertical direction)

where P_{t1} and P_{t2} are measured tensile forces of the top post-tensioning steel bar, P_{b1} and P_{b2} are measured tensile forces of the bottom post-tensioning steel bar, C_{c1} and C_{c2} are concrete compressive resultant forces and V_c is the measured story shear force. Joint shear strength for Specimens BHH2 and BHH3 which were computed by Equation (2) agreed well with average strength predicted by AIJ provisions [1]. For these specimens failing in joint panel, joint shear force reached the strength at the joint shear distortion of 2% after story shear force attained the maximum. For Specimens BNN1, BHH1 and BFH which failed eventually in joint shear after the post-tensioning steel bars yielded, joint shear force was less than average strength, but agreed approximately with lower strength by AIJ provisions [1].

For Specimen BNN2 whose initial tensile force imposed to post-tensioning steel bars was almost the half of the control Specimen BNN1 and which failed by yielding of the post-tensioning steel bars after concrete crushing at beam ends in bending moment, joint shear force also attained the lower predicted strength. Considering that joint panel was damaged severely and joint shear distortion attained 1.5%, this specimen is supposed to have failed in joint shear. For Specimen BNU which failed by concrete flexural compression at beam ends, joint shear force continued to increase even during keeping story shear force almost constant.

It is noted that the overlapping of concrete stress blocks on beam critical sections, which are opposed to each other across a joint panel, should be considered when joint input shear is computed in tests.

Joint Input Vertical Shear Force

Envelope curves of relationship between joint input vertical shear stresses and shear distortion are shown in Fig.9 by solid lines. The method to calculate joint input vertical shear force is identical with that of input horizontal shear force. In other words, joint input vertical shear force was computed in consideration of overlapping of the concrete compressive stress blocks on column critical sections (See Fig.11). Sectional area effective to vertical joint shear force was assumed as the product of beam depth and the average of beam and column width when input vertical shear force was transformed into shear stress.

The depth of concrete compressive stress block, which was not measured in tests, was obtained by the section analysis on the basis of the assumption that plane sections remain plane.

1) In case that depth of compressive stress block is less than the half of column depth;

$$V_{jv} = {}_C P_{L1} + {}_C P_{R2} + N - V_B \quad (7)$$

2) In case that depth of compressive stress block is greater than the half of column depth;

$$V_{jv} = {}_C P_{R1} + {}_C P_{R2} + \alpha_{3C} C_1 - \alpha_{4C} C_2 - V_B \quad (8)$$

$$ {}_C C_1 = {}_C P_{L1} - {}_C P_{R1} + N \quad (9)$$

$$ {}_C C_2 = {}_C P_{R2} - {}_C P_{L1} + N \quad (10)$$

$$ \alpha_3 = 1 - \alpha_4 \quad (11)$$

$$ \alpha_4 = (a_c - B/2)^2 / a_c^{\,2} \qquad (\alpha_3 + \alpha_4 = 1) \quad (12)$$

where ${}_C P_{R1}$ and ${}_C P_{L1}$ are tensile forces of column steel bar at top section, ${}_C P_{R2}$ and ${}_C P_{L2}$ are the tensile forces of column steel bar at bottom section, ${}_C C_1$ and ${}_C C_2$ are concrete compressive resultant forces, V_B is the beam shear force and N is an axial force as shown in Fig.11. Input vertical shear stress increased with the increase in joint shear distortion. The maximum input vertical shear stress of specimens BNN2 and BNU that did not fail in joint shear were from 12.5% to 30% less than specimens that failed in joint shear. Input vertical shear stress was almost equal to horizontal shear stress for all specimens except for Specimen BNN2.

Input vertical and horizontal shear stress was $0.70\sigma_B$ and $0.75\sigma_B$ respectively for interior beam-column joints, and $0.58\sigma_B$ and $0.79\sigma_B$ respectively for an exterior beam-column joint. Present shear design for beam-column joints limits only input horizontal shear force. It is recommended that joint shear design should be carried out allowing for both input horizontal and vertical shear force.

Diagonal Shear Crack Strength in Joint Panel

Diagonal shear crack strength in a joint panel (τ_{cr} : MPa) was obtained by Equation (13) based on the principal stress field taking account of the prestress to a beam (σ_p : $\sigma_p < 0$) and the axial compressive stress to a column(σ_0 : $\sigma_0 < 0$).

$$\tau_{cr} = \sqrt{f_t^{\,2} - (\sigma_0 + \sigma_p) f_t + \sigma_0 \sigma_p} \quad (13)$$

where f_t is a concrete tensile strength.

The depth of compressive stress block on the beam critical sections was greater than the half of beam depth at joint shear cracking except for Specimen BNN2. Therefore, the joint input shear force calculated by Equation (2) is compared with the computed strength. The joint input shear forces at positive and negative loading are shown in Fig.12. Joint shear crack strength in positive loading was almost equal to that in negative loading except for Specimen BHH2. Joint shear crack strength for Specimen BNN2 was smaller than that for other specimens. The comparisons between test results and calculations are shown in Table 6, where shaded column displays the ratio of calculation to test result. Joint input shear force in tests was taken as an average between the positive and negative loading. Joint shear stress was computed by dividing the joint input shear force by the column gross sectional area. Diagonal shear cracks in a joint panel are observed through the cover concrete in tests. Therefore, the column gross sectional area was

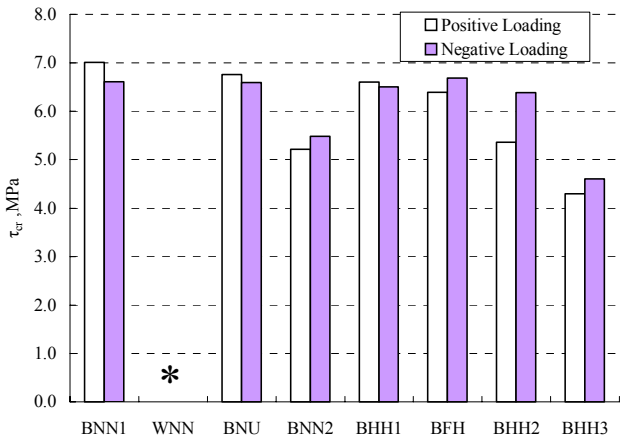

Fig.12 The joint input shear forces at positive and negative loading

Table 6 Diagonal shear crack strength in joint panel

Specimens	Measured result(MPa)	Computed result(MPa)	Ratio of computed to measured result
BNN1	6.81	11.06	1.62
WNN	- *	9.68	-
BNU	6.68	11.13	1.67
BNN2	5.35	9.35	1.75
BHH1	6.56	11.01	1.68
BFH	6.54	10.69	1.63
BHH2	5.87	8.33	1.42
BHH3	4.45	8.27	1.86
Average			***1.66***

**) The strain of prestressing strand in Specimen WNN could not be measured.*

considered to be effective on shear resistance in elastic region. The prestressing stress induced in beams was calculated from the product of column width and beam depth. The average ratio of calculated shear crack strength to measured shear stress was 1.66.

Since the shape of the shear stress distribution on rectangular section becomes the parabola on the basis of elastic theory, the maximum joint shear stress is obtained at the center of the section. Equation (13) was derived from the stress field of infinitesimal element on which shear stress acts uniformly. Accordingly, shear stress (τ_{cr}) in Equation (13) is equivalent to maximum shear stress at the center of joint panel. As the ratio of the average shear stress to maximum shear stress on rectangular section is 2/3 in elastic theory, the shear stress (τ_{cr}) in Equation (13) was multiplied by 2/3 to be changed to the average shear stress in joint panel. Consequently, the test results were almost equal to the computed results which were multiplied by 2/3.

Location of Compressive Resultant Forces at Beam Critical Section

Specimens BHH1, BNU, and BHH2 which showed different failure modes respectively, are used in following discussion.

With the aim of understanding the stress condition around beam-column joint panel, the position of the concrete compressive resultant force on a beam critical section was computed using tensile forces of post-tensioning steel bars and beam bending moment calculated from measured beam shear. The transition of location of compressive resultant forces, tensile resultant forces and lever arm length are shown in Fig13. The specific examples at the story drift angle of 2% are shown in Fig.14. Compressive resultant forces were located between top post-tensioning steel bar and the extreme compression fiber for all specimens. The lever arm lengths changed from 0.3d to 0.6d (d: 330mm). Lever arm length on prestressed beam section was shorter than that on RC sections because the tensile resultant force of top and bottom post-tensioning steel bars was located near the center of beam section during a test. The reason why the story shear forces declined after the strength is that tensile resultant force was kept constant after the post-tensioning steel bars yielded, whereas the lever arm length gradually decreased as shown in Fig.13.

Bond along Beam Post-tensioning Steel Bars

The average bond stresses along a beam post-tensioning steel bars within a joint for Specimens BHH1, BHH2 and BHH3 are shown in Fig.15. The average bond stress was computed by the difference between beam post-tensioning steel bar forces at opposite column faces. Bond stress of 1.0MPa for Specimen BHH2 was kept to the story drift angle of 1.5% and decreased whereas the tensile force of beam post-

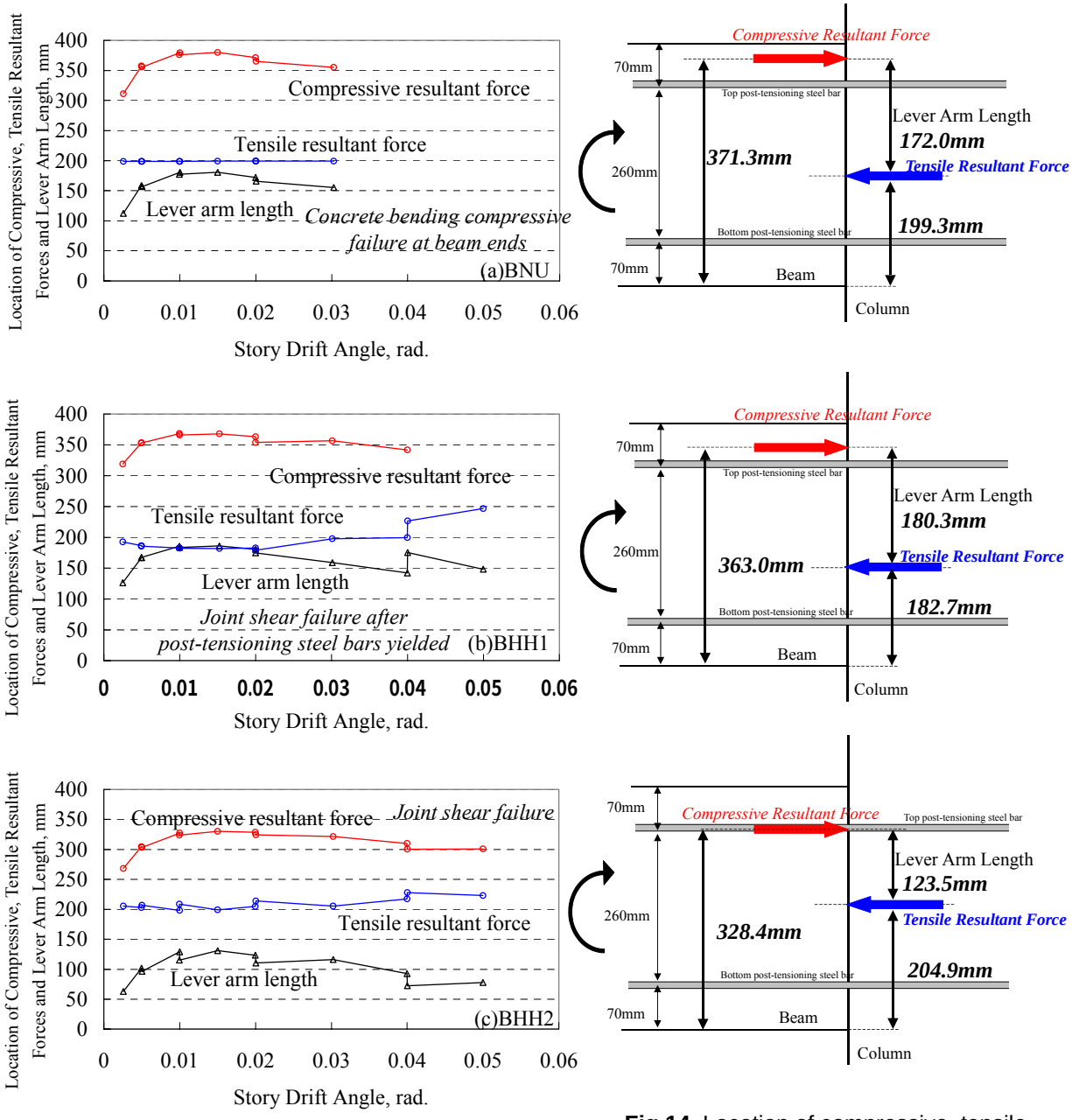

Fig.13 Transitions of location of compressive, tensile resultant forces and lever arm length on beam critical section

Fig.14 Location of compressive, tensile resultant forces and lever arm length at story drift angle of 2%

tensioning steel bars at critical sections increased to the story drift angle of 3.0%. It is judged that the decrease in bond stress along beam post-tensioning steel bars within a joint panel resulted from bond deterioration. The bond strength for Specimen BHH1 was greater than that for other specimens since high strength concrete was cast for the column. The bond deteriorated before the story shear forces reached the maximum for all specimens.

Deformation in Joint Panel

The lateral and vertical average strains in a joint panel are shown in Figs.16 and 17, respectively. These strains were computed by using average displacements measured by two horizontal and vertical

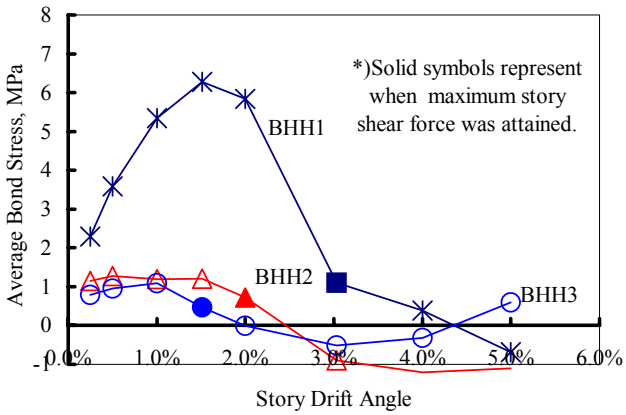

Fig.15 Average bond stress along beam post-tensioning steel bars within joint

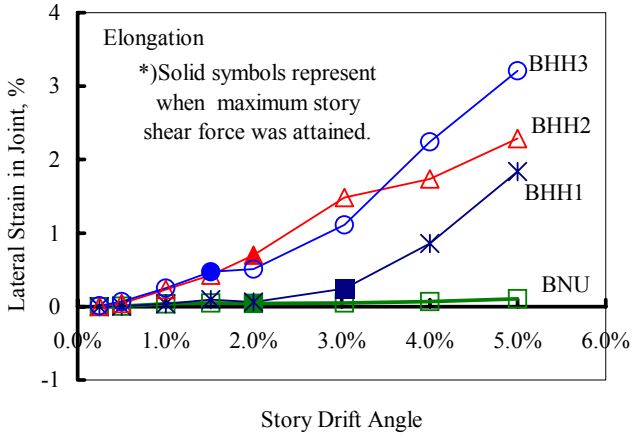

Fig.16 Lateral average strain in joint panel

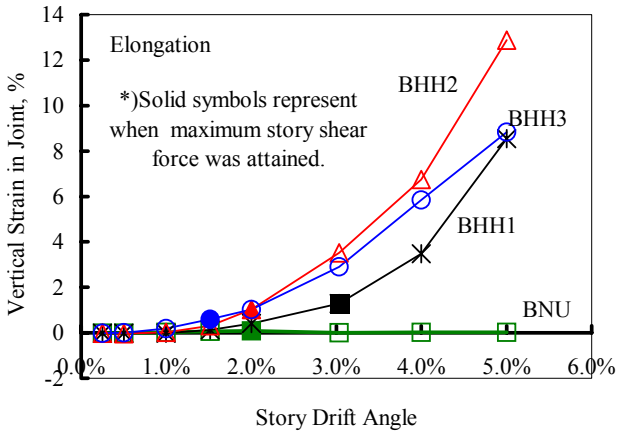

Fig.17 Vertical average strain in joint panel

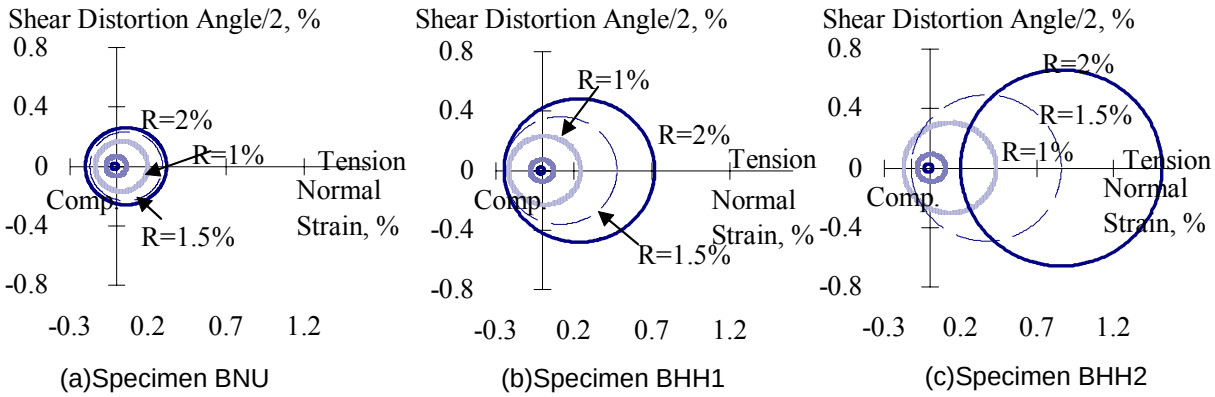

Fig.18 Mohr's strain circles for joint panel

displacement transducers. Both lateral and vertical average tensile strains kept increasing after the story shear forces reached the maximum for all specimens. Both average strains were negligible for Specimen BNU, which did not fail in joint shear.

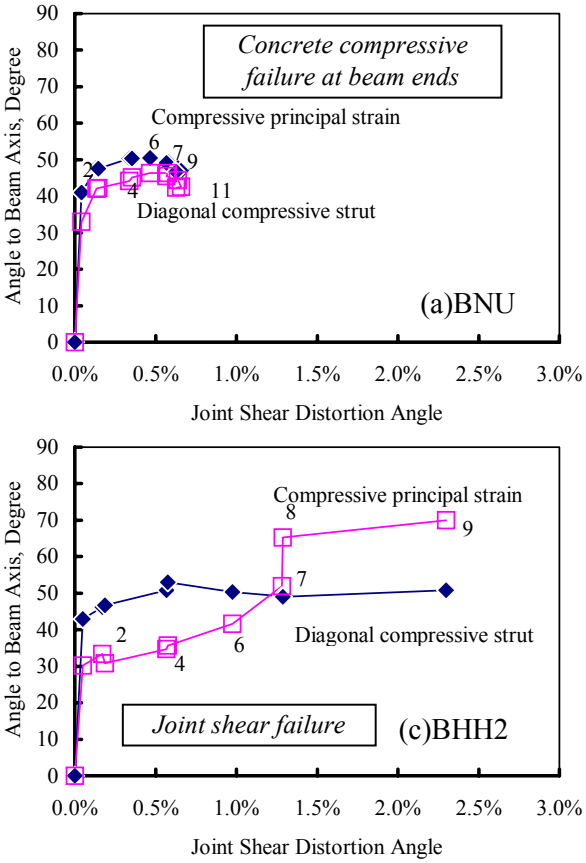

Fig.19 Angle of compressive principal strain and diagonal strut in joint panel

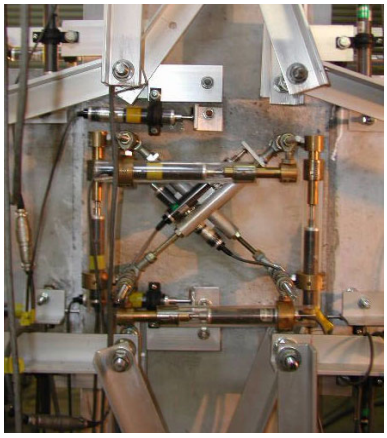

Fig.20 Instrumentation for joint panel distortion

Mohr's strain circles are shown in Fig.18 to the story drift angle of 2% to investigate deformation characteristics of a joint panel in more detail. The larger Mohr's circle is, the severer the damage in a joint panel is. The strain circles of Specimens BHH2 and BHH3 which failed in joint shear were larger than that for Specimen BNU. Centers of circle shifted largely to the tensile side. This indicates that the concrete in a joint panel expanded isotropically with the increase in a story drift. Joint shear failure for both specimens was caused by the concrete expansion. The strain circle for Specimen BNU that did not fail in joint shear was small. Center of circle was located near the origin and the Mohr's strain circle became large like as concentric circles.

Angle of Compressive Principal Strain and Diagonal Strut in Joint Panel

The angles of compressive principal strain and diagonal compressive strut to beam axis are shown in Fig.19. The arctangent of input horizontal and vertical shear force was deemed the angle of compressive strut in a joint panel. The angle of compressive principal strain was computed by using average strains measured by two horizontal, vertical and diagonal displacement transducers respectively as shown in Fig.20. The angle of diagonal compressive strut was nearly 50-degree regardless of joint shear deformation. In contrast, the angle of compressive principal strain increased from 35-degree to 85-degree with the increase in deformation. Both angles for Specimen BNU were identical to each other. Both angles for Specimens BHH1 and BHH2 were almost same until joint shear distortion of 0.7%. Hence diagonal compressive strut was formed in the same direction as compressive principal strain. However, the angle of compressive principal strain became larger than that of diagonal compressive strut after joint shear distortion of 0.5%, because joint lateral bars yielded and the shear cracks extended radically.

CONCLUSIONS

The following conclusions can be drawn from the present study:

(1) Interior and exterior beam-column joints which were made of assembling precast RC beams and column through post-tensioning steel bars failed in shear.

(2) The depth of compressive stress block obtained from the concrete strains at beam critical section was larger than the half of beam depth. This indicates that the joint panel concrete in central height was subjected to horizontal compression by concrete stress blocks on beam critical sections on both sides of a joint. Therefore all concrete compressive force on beam critical section did not necessarily contribute to joint input shear.

(3) The joint input shear force was computed by using the measured tensile forces of post-tensioning steel bars and considering that two concrete compressive stress blocks on opposite beam critical sections of a joint panel overlapped as mentioned above.

(a) Joint shear force reduced with the decrease in story shear force after the joint panel failed in shear.

(b) Shear strength of PCaPC beam-column joints can be estimated by the prediction method for usual RC beam-column joints.

(4) The measured joint shear cracking strength was almost equal to predicted strength by Equation (13) multiplied by 2/3.

(5) Since joint shear force is carried through diagonal compressive strut formed in joint core concrete, both horizontal and vertical shear forces imposed to a joint panel should be considered in joint shear design.

(6) Diagonal compressive strut was formed in the same direction as compressive principal strain. The angle of compressive principal strain became larger than that of diagonal compressive strut after joint shear distortion of 0.5%, because the joint lateral bars yielded and the shear cracks extended radically. The joint shear failure was caused by the expansion of joint core concrete.

REFERENCES

1. Architectural Institute of Japan, Design Guideline for Earthquake Resistant Reinforced Concrete Buildings Based on Inelastic Displacement Concept, 1999.
2. Beniya, N., Kashiwazaki, T. and Noguchi, H. : An Experimental Study on Shear Behavior of Prestressed Concrete Beam-Column Connection, Proceedings of JCI, Vol.19, No.2, pp.1179-1184, 1997.
3. Architectural Institute of Japan, Standard for Structural Design and Construction of Prestressed Concrete Structures, 1998.
4. Architectural Institute of Japan, Design Method of Prestressed (Reinforced) Concrete Structural Members -Actual Situation and Future, 2000.4